NONLINEAR CONTROL OF A FLEXIBLE ROTOR MAGNETIC BEARING SYSTEM: ROBUSTNESS AND THE INDEFINITE MODEL

Russell D. Smith
Department of Mechanical Engineering

William F. Weldon
Department of Mechanical Engineering
and
Department of Electrical and Computer Engineering

The University of Texas at Austin
Austin, Texas

ABSTRACT

Previously published control strategies for magnetic bearings primarily focus on linear optimal control techniques. While these methods afford many advantages, conspicuously absent from the literature are detailed attempts at nonlinear control. Here, we obtain the equations of motion of an overhung flexible rotor supported in magnetic bearings with two different levels of model sophistication. We derive a generic nonlinear controller in the manner of feedback linearization, and compare the eigenanalysis and transient response of the two rotor models under the action of this "perfect model" controller. We then proceed to obtain a robust nonlinear controller through the sliding mode technique and demonstrate that robustness by implementing it on an uncertain model.

INTRODUCTION

Magnetic bearings have been receiving increasing attention recently, and a wide spectrum of literature exists in the field (Geary, 1963, Humphris, 1985). Much of the literature which discusses control topics concentrates on linear optimal control techniques (references [7], [9], [10], [14], [18]). Linearizing the dynamics of magnetic bearing systems about the bearing center at a nominal speed affords opportunities for linear quadratic Gaussian optimal control. Since much of contemporary engineering activity appears to be directed at synthesis and optimization of the design process, linear techniques are justifiably popular. Maslen (1991) provides an excellent discussion of this synthesis in magnetic bearing design. Indeed, Burrows et. al. (1988) posit that linearized systems "...can be justified on the basis that there is a large body of knowledge to aid in the design of linear control systems but the design of nonlinear systems is still less well-defined."

As a practical matter, the issue appears to be not so much concerned with the possibility of a viable nonlinear controller, as with an adequate nonlinear observer. In general, nonlinear control laws frequently require full state feedback. For real systems, this is often a great hindrance, as many of the states either cannot effectively be measured, or can only be measured at great cost and inconvenience. Thus, the prob-lem evolves into one of designing an effective controller/observer combination, and this is elegantly provided by linear control theory. The well known *separation principle* of linear systems provides for closed loop system stability when the poles of the controller and the observer are independently stable (Kailath, 1980). This, of course, means that the observer and the controller can be designed independently, and the combination is assured to be stable. This principle, however, is predicated on linear dynamics, and is not necessarily applicable to nonlinear systems, in the general case. Nevertheless, much research has been done to address nonlinear observer design in an effort to make nonlinear compensators applicable to a wider class of problems (Slotine et. al. 1987, Raghavan, 1992, Raghavan and Hedrick, 1990).

Still, one wonders what advantages (or, disadvantages) might result from implementing nonlinear controllers on these increasingly popular bearing systems. Pradeep and Gurumoorthy (1993) have discussed the issue at one level, but we hope to provide a more explicit examination here. Specifically, we focus on the robustness of nonlinear control as provided by the sliding mode technique. Flexible system modelling, of course, may be done at different levels of sophistication, guided in part by the frequency range within which one expects the model to be accurate or useful. Real systems, behaving as a continuum, exhibit resonant phenomena beyond the highest mode modelled as the range of validity of a given model is exceeded. Thus, unmodelled dynamics are a key source of uncertainty with which control systems must contend. We will pursue nonlinear controller robustness in magnetic bearing systems by postulating a fairly simple flexible rotor system. This rotor will be modelled at increasing levels of sophistication, and nonlinear controllers will be designed to maintain the shaft centered in the bearings. We will then compare the eigenanalysis and transient response of this flexible rotor under the assumption of a "perfect model" (i.e., no uncertainty). Finally, in an effort to address this uncertainty, we will derive a robust nonlinear controller based on the crude rotor model, but implement that controller on the more sophisticated model. Thus, we hope to gain insight regarding the performance of a given nonlinear controller on a real system.

DYNAMIC MODEL

A generic flexible horizontal rotor supported in controlled dc electromagnetic bearings is shown in Figure 1. For the present discussion, we will assume a four pole bearing structure as indicated. More importantly, we will also assume that these magnetic actuators are current-
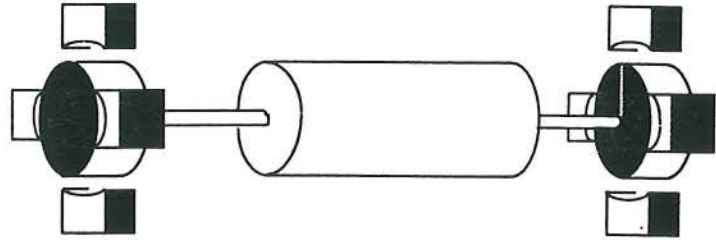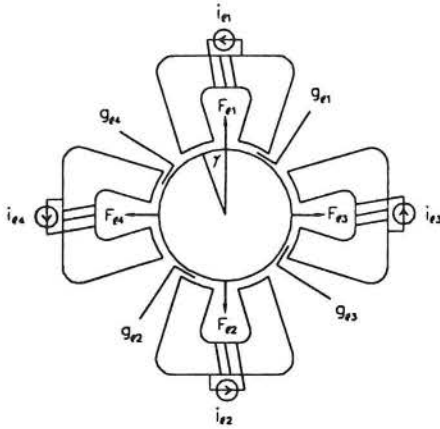
FIGURE 1: GENERIC MAGNETIC BEARING SYSTEM (4 POLE BEARING STRUCTURE, CURRENT-DRIVEN)
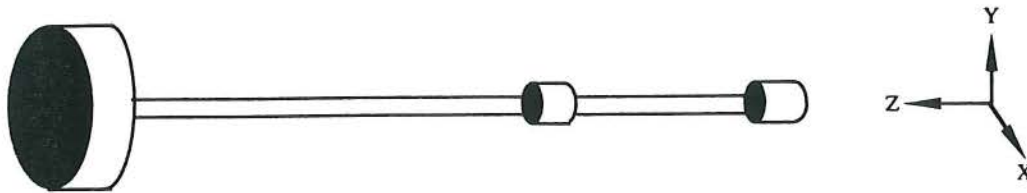

FIGURE 2: PHYSICAL SYSTEM MODEL OF INTEREST

driven. Thus the control effort will appear explicitly in the dynamics of the rotor, obviating the need of accounting for the electrical dynamics more accurately. This was done in order to simplify the mathematical treatment for the sake of clarity. Additionally, it is assumed that the magnetic actuator forces will be applied at discrete points on the shaft journals. This is tantamount to assuming that the pole face area of the electromagnets subtends a "small" fraction of the cylindrical journal surface area, and this assumption is in keeping with contemporary treatments. Furthermore, any eddy current force contributions will be assumed to be suppressed through the laminated journals attached to the shaft. Hebbale (1985) and Yoshimoto (1983) both discuss the analytical treatment of the eddy current effect in controlled electromagnetic bearings. In Figure 1, the axially controlled electromagnets (thrust bearing) are not shown. In the development that follows, we will refer to the bearings as "left" and "right", and physical variables at each location will be so designated. We now present as our physical system the overhung rotor shown in Figure 2. The overhung "disk" in Figure 2 might represent the impeller of some high speed device of interest. We will employ the fixed reference frame indicated in Figure 2 to express the dynamics of the rotor.

Two popular methods of flexible system modelling, of course, are the lumped parameter approach and the finite element techniques, and either of these strategies could serve our purposes here. The lumped parameter approach offers the advantage of maintaining a diagonal mass matrix in the equations of motion, and this simplifies the mathematics of the controller development somewhat, since we avoid coupling in the highest derivatives (i.e., as opposed to finite element techniques which yield a full mass matrix). We will postpone comment about the finite element models and proceed with the lumped parameter approach. We will adopt the notation of Childs (1993) and state the equations of motion in the fixed reference frame. Thus, we consider rigid body i with body-fixed (local) axes x_i, y_i, z_i where the z_i axis is the nominal axis

of symmetry. Vector $\underline{R}_i$ locates the origin of the x_i, y_i, z_i frame in the inertial frame X, Y, Z. Vector $\underline{a}_i$ locates the mass center of the rigid body in the x_i, y_i, z_i frame. Finally, we have the Z axis as the nominal spin axis of the rotor, and that rotation will be designated by the angular variable ϕ (taken positive in the positive Z direction). Assuming that our rotor is restrained from translating in the Z direction, we are interested in the R_{iX}, R_{iY} components of the displacement vector $\underline{R}_i$. The linear momentum principle yields:

$$m_i \ddot{R}_{iX} = f_{iX} + \hat{f}_{iX} + m_i a_{iX} \dot{\phi}^2 + m_i a_{iY} \ddot{\phi} \tag{1}$$

$$m_i \ddot{R}_{iY} = f_{iY} + \hat{f}_{iY} + m_i a_{iY} \dot{\phi}^2 - m_i a_{iX} \ddot{\phi} \tag{2}$$

where $\begin{bmatrix} a_{iX} \\ a_{iY} \end{bmatrix} = \begin{bmatrix} \cos\phi & -\sin\phi \\ \sin\phi & \cos\phi \end{bmatrix} \begin{bmatrix} a_{ix} \\ a_{iy} \end{bmatrix}$

are the fixed frame components of the mass imbalance vector, and we take $a_{iz} = 0$, which assumes that the x_i, y_i, z_i frame is oriented such that the center of mass of rigid body i is located in the x_i-y_i plane. f_{iX}, f_{iY} and $\hat{f}_{iX}, \hat{f}_{iY}$ are the components, respectively, of the external and the elastic reaction forces acting on rigid body i. Included in f_{iX}, f_{iY} will be the active bearing forces and dissipative terms. The angular degrees of freedom will be designated by the angles β_{iY}, β_{iX} which are rotations of the rigid body about the Y, X axes respectively. We have (neglecting second-order terms in the "small" angles):
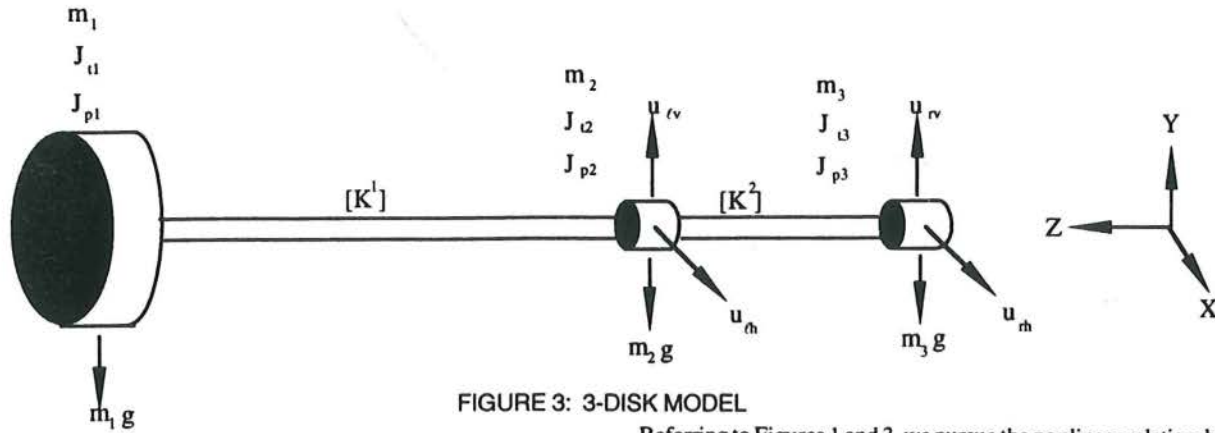
$$J_{ti}\ddot{\beta}_{iY} = M_{iY} + \hat{M}_{iY} + \dot{\phi}J_{pi}\dot{\beta}_{iX} + \dot{\phi}^2 J_{iXZ} + \ddot{\phi}J_{iYZ} \qquad (3)$$

$$J_{ti}\ddot{\beta}_{iX} = M_{iX} + \hat{M}_{iX} - \dot{\phi}J_{pi}\dot{\beta}_{iY} - \dot{\phi}^2 J_{iYZ} + \ddot{\phi}J_{iXZ} \qquad (4)$$

where $\begin{bmatrix} J_{iXZ} \\ J_{iYZ} \end{bmatrix} = \begin{bmatrix} \cos\phi & -\sin\phi \\ \sin\phi & \cos\phi \end{bmatrix}\begin{bmatrix} J_{ixz} \\ J_{iyz} \end{bmatrix}$

are the fixed frame products of inertia. J_{ti}, J_{pi} are, respectively, the transverse and polar moments of inertia. In equations (3) and (4), we have assumed an axially symmetric rigid body since we have not distinguished the transverse moments of inertia about the fixed frame axes.

Analogously with equations (1) and (2), M_{iX}, M_{iY} and $\hat{M}_{iX}, \hat{M}_{iY}$ represent the external and elastic reaction moments of the rigid body about the designated axes. We will assume torsional rigidity and express our final degree of freedom with the axial rotation equation of motion:

$$\bar{J}\ddot{\phi} = \sum_i M_z + \sum_i (J_{iXZ}\ddot{\beta}_{iX} + J_{iYZ}\ddot{\beta}_{iY})$$
$$- \sum_i M_i(a_{iX}\ddot{R}_{iY} - a_{iY}\ddot{R}_{iX}) \qquad (5)$$

where $\bar{J} = \sum_i (J_{pi} + m_i|a_i|^2)$

We will employ body-fixed (local) axes coincident with principal axes such that our fixed frame products of inertia vanish. For modest translational accelerations and unbalance vectors, the third term of equation (5) will not substantially affect the analysis, and we may therefore approximate equation (5) with:

$$\bar{J}\ddot{\phi} = \sum_i M_z \qquad (6)$$

The elastic reaction forces acting on adjacent rigid bodies in the X-Z plane will be taken from the stiffness matrix definitions as follows (Lalanne and Ferraris, 1990):

$$\begin{bmatrix} \hat{f}_{1X} \\ \hat{M}_{1Y} \\ \hat{f}_{2X} \\ \hat{M}_{2Y} \end{bmatrix} = -\begin{bmatrix} K_{11} & K_{12} & K_{13} & K_{14} \\ K_{21} & K_{22} & K_{23} & K_{24} \\ K_{31} & K_{32} & K_{33} & K_{34} \\ K_{41} & K_{42} & K_{43} & K_{44} \end{bmatrix}$$

$$= -\frac{2EI}{L^3}\begin{bmatrix} 6 & 3L & -6 & 3L \\ 3L & 2L^2 & -3L & L^2 \\ -6 & -3L & 6 & -3L \\ 3L & L^2 & -3L & 2L^2 \end{bmatrix}\begin{bmatrix} R_{1X} \\ \beta_{1Y} \\ R_{2X} \\ \beta_{2Y} \end{bmatrix} \qquad (7)$$

and for a flexibly symmetric rotor, we will use the same elastic definitions for the Y-Z plane in the analagous terms $\begin{bmatrix} \hat{f}_{1Y} & \hat{M}_{1X} & \hat{f}_{2Y} & \hat{M}_{2X} \end{bmatrix}^T$. The stiffness matrix above refers, of course, to two rigid bodies with elastic forces from only one intervening beam element. For the general case of a series of rigid members compliantly connected, we will employ the notational convenience

from Childs (1993) and refer to each stiffness matrix with a superscript. Thus, for three rigid bodies joined by two elastic elements:

$$\begin{bmatrix} \hat{f}_{1X} \\ \hat{M}_{1Y} \\ \hat{f}_{2X} \\ \hat{M}_{2Y} \\ \hat{f}_{3X} \\ \hat{M}_{3Y} \end{bmatrix} = -[K]\begin{bmatrix} R_{1X} \\ \beta_{1Y} \\ R_{2X} \\ \beta_{2Y} \\ R_{3X} \\ \beta_{3Y} \end{bmatrix} \qquad (8)$$

$$[K] = -\begin{bmatrix} K^1_{11} & K^1_{12} & K^1_{13} & K^1_{14} & 0 & 0 \\ K^1_{21} & K^1_{22} & K^1_{23} & K^1_{24} & 0 & 0 \\ K^1_{31} & K^1_{32} & (K^1_{33}+K^2_{33}) & (K^1_{34}+K^2_{34}) & K^2_{35} & K^2_{36} \\ K^1_{41} & K^1_{42} & (K^1_{43}+K^2_{43}) & (K^1_{44}+K^2_{44}) & K^2_{45} & K^2_{46} \\ 0 & 0 & K^2_{53} & K^2_{54} & K^2_{55} & K^2_{56} \\ 0 & 0 & K^2_{63} & K^2_{64} & K^2_{65} & K^2_{66} \end{bmatrix}$$

where each 4x4 component of the banded matrix is as defined in equation (7). As we have already mentioned, we will assume a symmetrical rotor and, therefore, we will be using an identical model stiffness matrix for motion in the Y-Z plane.

3-DISK MODEL

Returning to our physical system shown in Figure 2, we consider the most crude lumped parameter representation and model it with the 3-disk approximation depicted in Figure 3. Here, the mass and inertia of the flexible beam elements have been divided equally between the adjacent rigid "disks". Employing equations (1) - (4) and (6), this 13 degree-of-freedom model may be expressed as:

$$\begin{bmatrix} [M] & 0 \\ 0 & [M] \end{bmatrix}\ddot{\underline{x}} + \begin{bmatrix} [C_D] & -[C_G] \\ [C_G] & [C_D] \end{bmatrix}\dot{\underline{x}} + \begin{bmatrix} [K] & 0 \\ 0 & [K] \end{bmatrix}\underline{x} = \underline{F} \qquad (9)$$

$$\bar{J}\ddot{\phi} = \sum_i M_z \qquad (10)$$

where

$$\underline{x} = [\underline{x}_{X-Z}\ \underline{x}_{Y-Z}]^T$$

$$= [R_{1X}\ \beta_{1Y}\ R_{2X}\ \beta_{2Y}\ R_{3X}\ \beta_{3Y}\ R_{1Y}\ \beta_{1X}\ R_{2Y}\ \beta_{2X}\ R_{3Y}\ \beta_{3X}]^T$$

$$[M] = \begin{bmatrix} m_1 & & & & & \\ & J_{t1} & & & 0 & \\ & & m_2 & & & \\ & & & J_{t2} & & \\ & 0 & & & m_3 & \\ & & & & & J_{t3} \end{bmatrix}$$

$$[C_D] = \begin{bmatrix} \alpha_1 & & & & & \\ & 0 & & & 0 & \\ & & \alpha_2 & & & \\ & & & 0 & & \\ & 0 & & & \alpha_3 & \\ & & & & & 0 \end{bmatrix}$$

FIGURE 3: 3-DISK MODEL

$$[C_G] = \begin{bmatrix} 0 & & & & & & \\ & \dot{\phi}J_{p1} & & & & 0 & \\ & & 0 & & & & \\ & & & \dot{\phi}J_{p2} & & & \\ & 0 & & & 0 & & \\ & & & & & \dot{\phi}J_{p3} & \end{bmatrix}$$

$$\underline{F} = \begin{bmatrix} m_1a_{1X}\dot{\phi}^2 + m_1a_{1Y}\ddot{\phi} \\ 0 \\ m_2a_{2X}\dot{\phi}^2 + m_2a_{2Y}\ddot{\phi} + u_{rh} \\ 0 \\ m_3a_{3X}\dot{\phi}^2 + m_3a_{3Y}\ddot{\phi} + u_{rh} \\ 0 \\ m_1a_{1Y}\dot{\phi}^2 - m_1a_{1X}\ddot{\phi} - m_1g \\ 0 \\ m_2a_{2Y}\dot{\phi}^2 - m_2a_{2X}\ddot{\phi} - m_2g + u_{\ell v} \\ 0 \\ m_3a_{3Y}\dot{\phi}^2 - m_3a_{3X}\ddot{\phi} - m_3g + u_{rv} \\ 0 \end{bmatrix}$$

and we have included $[C_D]$ to reflect translational damping, but have not labored to include terms owing to transverse rotational damping. Remaining external forces primarily include the magnetic bearing forces which we have combined as pseudoinputs (**u**'s), or the net vertical and horizontal actuator forces at the left and right bearings. The assumed positive direction of these pseudoinputs is also indicated in Figure 3. Since we had chosen local frame axes to coincide with principal axes, all terms owing to products of inertia vanished from equations (3) and (4), and are therefore not present in the external force vector above. Neither do we choose to represent any other external moments. In some real device, of course, one would model fluid interaction forces, seals, couplings, etc. The stiffness submatrix [K] in equation (9) is as defined by (8), where, obviously, the geometry and material properties (i.e., E, I, L) are, in general, unique for each element. We will defer the eigenanalysis of this 3-disk model until we have specified our control functions.

ACTUATOR FORCE RELATIONSHIPS

Referring to Figures 1 and 3, we pursue the nonlinear relationships that comprise the bearing forces and begin with the magnetic energy expression (Woodson and Melcher, 1990, or Sortore, 1990)):

$$W_m = \oint_v \frac{1}{2\mu} B^2 dv$$

where $\mu = \mu_r\mu_o$, and v is a volume of interest

We will neglect leakage and fringing in this simplified model, and assume that, in the air gaps, iron paths, and journal, the magnetic flux and flux density are constant. Also, the iron will be treated as operating below saturation; we will further assume that it is behaving linearly in this region. We examine a single electromagnet for which the cross section of the flux paths will be approximated as remaining constant in each medium.

$$W_m = \oint_v \frac{1}{2\mu} B^2 dv = \frac{B^2}{2\mu_0} \left[2g + \frac{\ell_{iron}}{\mu_{iron}} + \frac{\ell_{journ}}{\mu_{journ}} \right] A_g \qquad (11)$$

$$MMF = NI = \Re\Phi$$

where $\Re, \Phi$ denote the magnetic reluctance and the magnetic flux in the paths, respectively

$$\Re = \frac{\ell_{path}}{\mu_o\mu_{r,path}A_{path}}$$

Under the assumption of no leakage,

$$\Phi_{gap} = \Phi_{iron} = \Phi_{journ} = \Phi$$

$$\Phi = \frac{NI}{\left[\dfrac{2g}{\mu_o} + \dfrac{\ell_{iron}}{\mu_o\mu_{iron}} + \dfrac{\ell_{journ}}{\mu_o\mu_{journ}} \right] \dfrac{1}{A_g}}$$

$$= \frac{\mu_o A_g NI}{\left(2g + \dfrac{\ell_{iron}}{\mu_{iron}} + \dfrac{\ell_{journ}}{\mu_{journ}} \right)} \qquad (12)$$

Now taking $B = \Phi / A_g$ and making the appropriate substitutions into equation (11),

$$W_m = \frac{\mu_o A_g N^2 I^2}{2\left(2g + \dfrac{\ell_{iron}}{\mu_{iron}} + \dfrac{\ell_{journ}}{\mu_{journ}}\right)} \tag{13}$$

from which the force acting on the rotor from the actuator may be determined,

$$F = \frac{\partial W_m}{\partial g}$$

$$
\begin{aligned}
F &= -\frac{\mu_o A_g N^2 I^2 (2)}{2\left(2g + \dfrac{\ell_{iron}}{\mu_{iron}} + \dfrac{\ell_{journ}}{\mu_{journ}}\right)^2} \\[2mm]
&= -\frac{\mu_o A_g N^2 I^2}{\left(2g + \dfrac{\ell_{iron}}{\mu_{iron}} + \dfrac{\ell_{journ}}{\mu_{journ}}\right)^2}
\end{aligned}
\tag{14}$$

The above expression is the sum of the two contributions of the actuator force directed along each axis of the pole faces. In general, this must be multiplied by the cosine of the angle between the axis of the actuator and the axis of a pole face. Therefore,

$$
\begin{aligned}
F_{\ell,i} &= -\frac{\mu_o A_g N^2 I_{\ell,i}^2 \cos\gamma}{\left(2g_{\ell,i} + \varepsilon\right)^2} = -\frac{K I_{\ell,i}^2}{\left(2g_{\ell,i} + \varepsilon\right)^2} \\[2mm]
&\approx -\frac{K_a I_{\ell,i}^2}{g_{\ell,i}^2}
\end{aligned}
\tag{15}$$

and

$$
\begin{aligned}
F_{r,i} &= -\frac{\mu_o A_g N^2 I_{r,i}^2 \cos\gamma}{\left(2g_{r,i} + \varepsilon\right)^2} = -\frac{K I_{r,i}^2}{\left(2g_{r,i} + \varepsilon\right)^2} \\[2mm]
&\approx -\frac{K_a I_{r,i}^2}{g_{r,i}^2}
\end{aligned}
\tag{16}$$

where we have written $\varepsilon = \dfrac{\ell_{iron}}{\mu_{iron}} + \dfrac{\ell_{journ}}{\mu_{journ}}$

Finally, we shall say that

$$
\begin{array}{ll}
u_{\ell h} = F_{\ell 3} - F_{\ell 4} & u_{rh} = F_{r3} - F_{r4} \\[2mm]
u_{\ell v} = F_{\ell 1} - F_{\ell 2} & u_{rv} = F_{r1} - F_{r2}
\end{array}
\tag{17}$$

We recognize that our neglect of fringing fields will be manifested in part by the inaccuracy of equation (16) as the gap length approaches both large and small characteristic dimensions. However, we are motivated to make use of this simplified actuator model by the knowledge that a real system would employ back-up bearings to assure finite gap length in case of power failure, etc. Further, our primary interest is to animate the discussion at hand, and equation (16) will be adequate at present.

CONTROLLER DESIGN (3-DISK MODEL)

For the case of the nonlinear *regulator* problem, we take Δ as the desired air gap length, and we write the expressions for the eight air gap lengths. Here, we recognize that an air gap length expression along a given axis is only a weak function of motion along a perpendicular axis for many practical geometries (Sortore, 1990). Thus,

$$
\begin{array}{ll}
g_{\ell 1} = \Delta - R_{2Y} & g_{r1} = \Delta - R_{3Y} \\
g_{\ell 2} = \Delta + R_{2Y} & g_{r2} = \Delta + R_{3Y} \\
g_{\ell 3} = \Delta - R_{2X} & g_{r3} = \Delta - R_{3X} \\
g_{\ell 4} = \Delta + R_{2X} & g_{r4} = \Delta + R_{3X}
\end{array}
\tag{18}$$

Obviously, these eight expressions are not all independent, and a minimum set of four will be needed. Selecting a vertical and horizontal gap length *error* on both the left and right bearings as our system outputs, these may be differentiated successively until the control pseudoinputs appear. Through this input-output linearization (Slotine and Li, 1991), the resulting equations may then be solved algebraically for the pseudoinputs such that:

i) the nonlinearities are cancelled
ii) exponentially stable, linear closed loop error dynamics are assured
iii) robustness is provided in the face of structured (parameter) uncertainty and/or unmodelled dynamics

Beginning with $\tilde{g}_{\ell 1}$, we obtain from the mathematical model of equations (9):

$$
\begin{aligned}
\tilde{g}_{\ell 1} &= g_{\ell 1} - \Delta \\
\tilde{g}_{\ell 1} &= -R_{2Y} \\
\dot{\tilde{g}}_{\ell 1} &= -\dot{R}_{2Y} \\
\ddot{\tilde{g}}_{\ell 1} &= -\ddot{R}_{2Y} = -(1/m_2)\{-\hat{f}_{2Y} - \alpha\dot{R}_{2Y} + m_2 a_{2Y}\dot{\phi}^2 \\
&\qquad\qquad\qquad - m_2 a_{2X}\ddot{\phi} - m_2 g + u_{\ell v}\}
\end{aligned}
$$

$$
\begin{aligned}
\tilde{g}_{\ell 3} &= g_{\ell 3} - \Delta \\
\tilde{g}_{\ell 3} &= -R_{2X} \\
\dot{\tilde{g}}_{\ell 3} &= -\dot{R}_{2X} \\
\ddot{\tilde{g}}_{\ell 3} &= -\ddot{R}_{2X} = -(1/m_2)\{-\hat{f}_{2X} - \alpha\dot{R}_{2X} + m_2 a_{2X}\dot{\phi}^2 \\
&\qquad\qquad\qquad + m_2 a_{2Y}\ddot{\phi} + u_{\ell h}\}
\end{aligned}
$$

5

$$\tilde{g}_{r1} = g_{r1} - \Delta$$

$$\tilde{g}_{r1} = -R_{3Y}$$

$$\dot{\tilde{g}}_{r1} = -\dot{R}_{3Y}$$

$$\ddot{\tilde{g}}_{r1} = -\ddot{R}_{3Y} = -(1/m_3)\{-\hat{f}_{3Y} - \alpha\dot{R}_{3Y} + m_3 a_{3Y}\dot{\phi}^2$$
$$- m_3 a_{3X}\ddot{\phi} - m_3 g + \mathbf{u}_{rv}\}$$

$$\tilde{g}_{r3} = g_{r3} - \Delta$$

$$\tilde{g}_{r3} = -R_{3X}$$

$$\dot{\tilde{g}}_{r3} = -\dot{R}_{3X}$$

$$\ddot{\tilde{g}}_{r3} = -\ddot{R}_{3X} = -(1/m_3)\{-\hat{f}_{3X} - \alpha\dot{R}_{3X} + m_3 a_{3X}\dot{\phi}^2$$
$$+ m_3 a_{3Y}\ddot{\phi} + \mathbf{u}_{rh}\}$$

Therefore, we choose our control functions as:

$$\mathbf{u}_{\ell v} = \{\hat{f}_{2Y} + \alpha\dot{R}_{2Y} - m_2 a_{2Y}\dot{\phi}^2 + m_2 a_{2X}\ddot{\phi} + m_2 g\}$$
$$+ m_2\{c_1\dot{\tilde{g}}_{\ell 1} + c_2\tilde{g}_{\ell 1}\}$$

$$\mathbf{u}_{\ell h} = \{\hat{f}_{2X} + \alpha\dot{R}_{2X} - m_2 a_{2X}\dot{\phi}^2 - m_2 a_{2Y}\ddot{\phi}\}$$
$$+ m_2\{c_1\dot{\tilde{g}}_{\ell 3} + c_2\tilde{g}_{\ell 3}\}$$

$$\mathbf{u}_{rv} = \{\hat{f}_{3Y} + \alpha\dot{R}_{3Y} - m_3 a_{3Y}\dot{\phi}^2 + m_3 a_{3X}\ddot{\phi} + m_3 g\} \qquad (19)$$
$$+ m_3\{c_1\dot{\tilde{g}}_{r1} + c_2\tilde{g}_{r1}\}$$

$$\mathbf{u}_{rh} = \{\hat{f}_{3X} + \alpha\dot{R}_{3X} - m_3 a_{3X}\dot{\phi}^2 - m_3 a_{3Y}\ddot{\phi}\}$$
$$+ m_3\{c_1\dot{\tilde{g}}_{r3} + c_2\tilde{g}_{r3}\}$$

where the reader is referred to equations (8) for the notational expansion of the elastic forces. In the control law(s) specified above, the first terms in braces represent the nonlinear cancellation, while the last terms provide for linear, exponentially stable closed loop error dynamics. For the sake of brevity, we shall refer to equations (19) as the I/O controller. Upon substitution of equations (19) into the error dynamics equations above, we see:

$$\ddot{\tilde{g}}_{\ell 1} + c_1\dot{\tilde{g}}_{\ell 1} + c_2\tilde{g}_{\ell 1} = 0$$

$$\ddot{\tilde{g}}_{\ell 3} + c_1\dot{\tilde{g}}_{\ell 3} + c_2\tilde{g}_{\ell 3} = 0$$

$$\ddot{\tilde{g}}_{r1} + c_1\dot{\tilde{g}}_{r1} + c_2\tilde{g}_{r1} = 0 \qquad (20)$$

$$\ddot{\tilde{g}}_{r3} + c_1\dot{\tilde{g}}_{r3} + c_2\tilde{g}_{r3} = 0$$

which implies $\tilde{g}$'s $\rightarrow 0$ as $t \rightarrow \infty$ provided that we guarantee positive feedback gains. We have chosen here to specify equally convergent error dynamics along each axis (i.e., X and Y) for both bearings, but in the general case, one might pursue another course of action. Furthermore, we will be selecting slightly overdamped roots in an effort to

avoid introducing possible resonant phenomena if the shaft speed should correspond to controller natural frequencies in the general case of an imperfect model. In other words, with model uncertainty, our nonlinear cancellation will be imperfect (the first terms of the control law(s) of (19)), and the physical system will respond as with terms on the r.h.s. of equations (20) which will be harmonic in the shaft speed as is evident from a_{iX}, a_{iY}.

From our definitions in equations (17) and the bearing force models in equations (15) and (16), we choose to specify the currents $I_{\ell,i}$, $I_{r,i}$ according to whether the control law in question requires positive or negative effort. Thus, only one of the vertical or horizontal electromagnet pairs is activated at a given time, and we recognize that this strategy is only one of many possible controller schemes. We now proceed with the eigenanalysis of our 3-disk model.

EIGENANALYSIS (3-DISK MODEL)

Proceeding conventionally, we substitute equations (19) into the mathematical model of equations (9) and consider the homogeneous vibration equations:

$$\begin{bmatrix} [M'] & 0 \\ 0 & [M'] \end{bmatrix}\ddot{\underline{x}} + \begin{bmatrix} [C_D'] & -[C_G] \\ [C_G] & [C_D'] \end{bmatrix}\dot{\underline{x}} + \begin{bmatrix} [K'] & 0 \\ 0 & [K'] \end{bmatrix}\underline{x} = \underline{0} \qquad (21)$$

or, $\qquad [M'']\ddot{\underline{x}} + [C'']\dot{\underline{x}} + [K'']\underline{x} = \underline{0} \qquad (22)$

where

$$\underline{x} = [\underline{x}_{X-Z}\ \underline{x}_{Y-Z}]^T$$

$$= [R_{1X}\ \beta_{1Y}\ R_{2X}\ \beta_{2Y}\ R_{3X}\ \beta_{3Y}\ R_{1Y}\ \beta_{1X}\ R_{2Y}\ \beta_{2X}\ R_{3Y}\ \beta_{3X}]^T$$

$$[M'] = \begin{bmatrix} m_1 & & & & & \\ & J_{t1} & & & 0 & \\ & & m_2 & & & \\ & & & J_{t2} & & \\ & 0 & & & m_3 & \\ & & & & & J_{t3} \end{bmatrix}$$

$$[C_D'] = \begin{bmatrix} \alpha_1 & & & & & \\ & 0 & & & 0 & \\ & & m_2 c_1 & & & \\ & & & 0 & & \\ & 0 & & & m_3 c_1 & \\ & & & & & 0 \end{bmatrix}$$

$$[C_G] = \begin{bmatrix} 0 & & & & & \\ & \dot{\phi}J_{p1} & & & 0 & \\ & & 0 & & & \\ & & & \dot{\phi}J_{p2} & & \\ & 0 & & & 0 & \\ & & & & & \dot{\phi}J_{p3} \end{bmatrix}$$

$$[K'] = \begin{bmatrix} K_{11}^1 & K_{12}^1 & K_{13}^1 & K_{14}^1 & 0 & 0 \\ K_{21}^1 & K_{22}^1 & K_{23}^1 & K_{24}^1 & 0 & 0 \\ 0 & 0 & m_2 c_2 & 0 & 0 & 0 \\ K_{41}^1 & K_{42}^1 & (K_{43}^1 + K_{43}^2) & (K_{44}^1 + K_{44}^2) & K_{45}^2 & K_{46}^2 \\ 0 & 0 & 0 & 0 & m_3 c_2 & 0 \\ 0 & 0 & K_{63}^2 & K_{64}^2 & K_{65}^2 & K_{66}^2 \end{bmatrix}$$
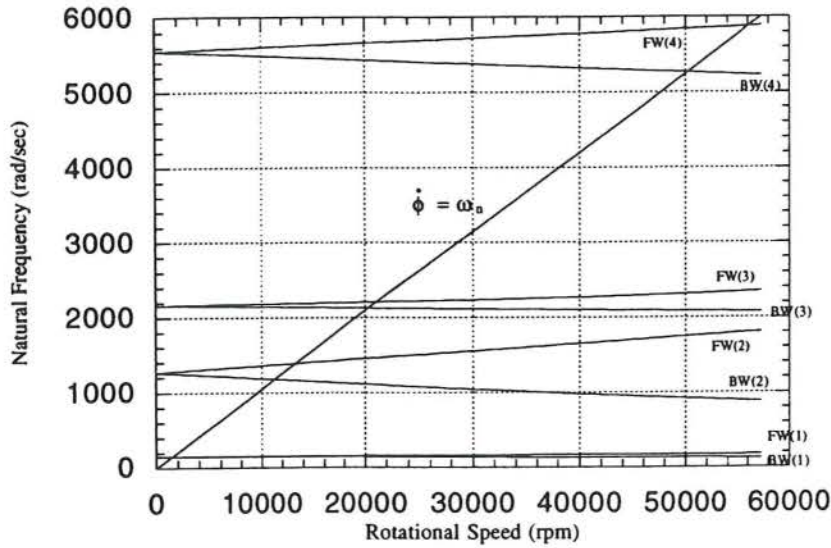
6

FIGURE 4: CAMPBELL DIAGRAM (3-DISK MODEL)

TABLE 1: 3-DISK MODEL PARAMETERS

L_1: .333 m	
D_1: .013 m	J_{p1}: .000121 kgm^2 J_{p2}: .00001 kgm^2 J_{p3}: 9×10^{-6} kgm^2
E_1: 70×10^9 Pa	J_{t1}: .000638 kgm^2 J_{t2}: .000657 kgm^2 J_{t3}: 7.9×10^{-9} kgm^2
I_1: 1.4×10^{-9} m^4	m_1: .228 kg m_2: .192 kg m_3: .130 kg
L_2: .167 m	
D_2: .013 m	a_{1x}: .000381 m a_{1y}: 0 α: 1.5 N $-$ sec/ m
E_2: 70×10^9 Pa	a_{2x}: $-$.000127 m a_{2y}: 0 Δ: .001 m c_1: 65
I_2: 1.4×10^{-9} m^4	a_{3x}: .000127 m a_{3y}: 0 K_a: 8×10^{-6} c_2: 1050

TABLE 2: 3-DISK MODEL FORWARD AND BACKWARD CRITICAL SPEEDS

Forward Synchronous Whirl	Backward Synchronous Whirl
ω_{cr1} = FW(1) = 148 rad/sec (1429 rpm)	ω_{cr1} = BW(1) = 148 rad/sec (1416 rpm)
ω_{cr2} = FW(2) = 1388 rad/sec (13,254 rpm)	ω_{cr2} = BW(2) = 1175 rad/sec (11,220 rpm)
ω_{cr3} = FW(3) = 2207 rad/sec (21,075 rpm	ω_{cr3} = BW(3) = 2126 rad/sec (20,302 rpm)

7
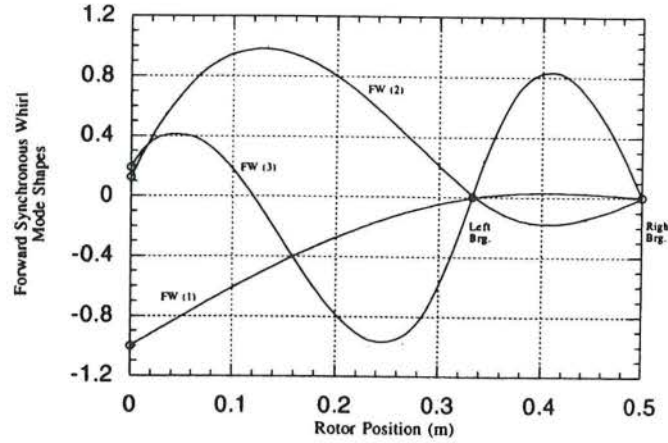
FIGURE 5: FORWARD SYNCHRONOUS WHIRL MODE SHAPES (3-DISK MODEL)
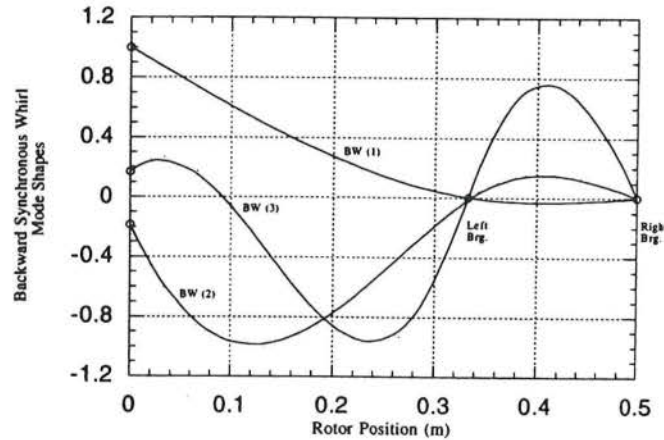
FIGURE 6: BACKWARD SYNCHRONOUS WHIRL MODE SHAPES (3-DISK MODEL)

Now, defining $\underline{\chi} = [\underline{\dot{x}} \; \underline{x}]^T$ and rewriting equation (22) in first-order eigenvalue form:

$$\begin{bmatrix} [M''] & [0] \\ [0] & [I] \end{bmatrix} \underline{\dot{\chi}} + \begin{bmatrix} [C''] & [K''] \\ -[I] & [0] \end{bmatrix} \underline{\chi} = \underline{0} \qquad (23)$$

The eigenvalues are given in the Campbell diagram in Figure 4 for the parameters specified in Table 1. The masses and inertias in Table 1 are the effective values at each of the three nodes. Since we assumed a symmetrically stiff rotor, we only examine the Y-Z (vertical) plane. From our original 12 degrees of freedom in equations (9), our feedback has decoupled the translational degrees at both bearing journals, thus leaving only 4 degrees of freedom per plane. This, of course, presumes perfect knowledge of the plant dynamics.

The first three forward and backward synchronous whirl critical speeds are given in Table 2, and the mode shapes for both forward and backward synchronous whirl are shown in Figures 5 and 6. These mode shapes have been sketched in with the aid of a cubic polynomial fitted between consecutive nodal points such that the slope and displacement boundary conditions (i.e., from the eigenvector) were satisfied. Obviously, the points corresponding to the bearings remain at zero displacement under the decoupling of our control law.

From the Campbell Diagram in Figure 4, the highest natural frequency is substantially greater than the lower three, and we should certainly expect that this crude 3-disk model will be inappropriate as we approach the highest natural frequency modelled. We therefore have not bothered to plot the fourth mode shape, as we will not be interested in the rotor response beyond 30-40000 rpm.

8
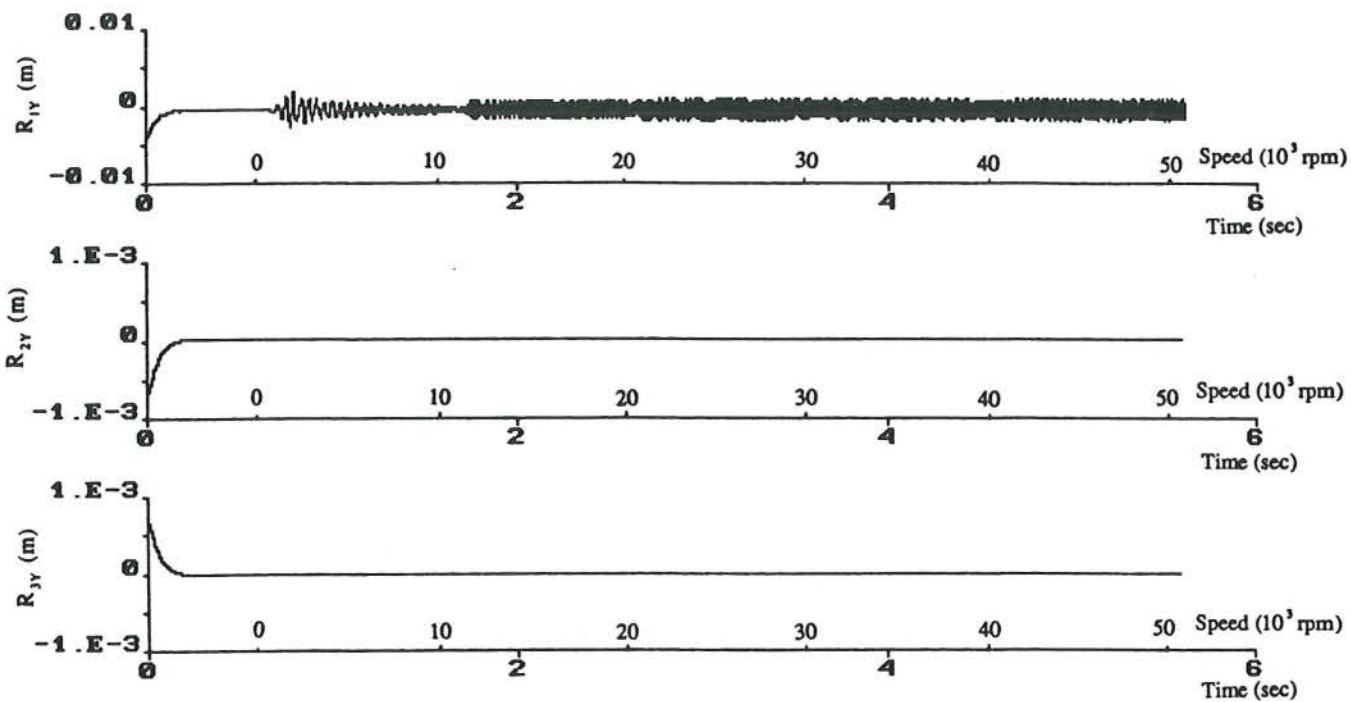
FIGURE 7: TRANSIENT RESPONSE DEFLECTIONS (3-DISK MODEL)
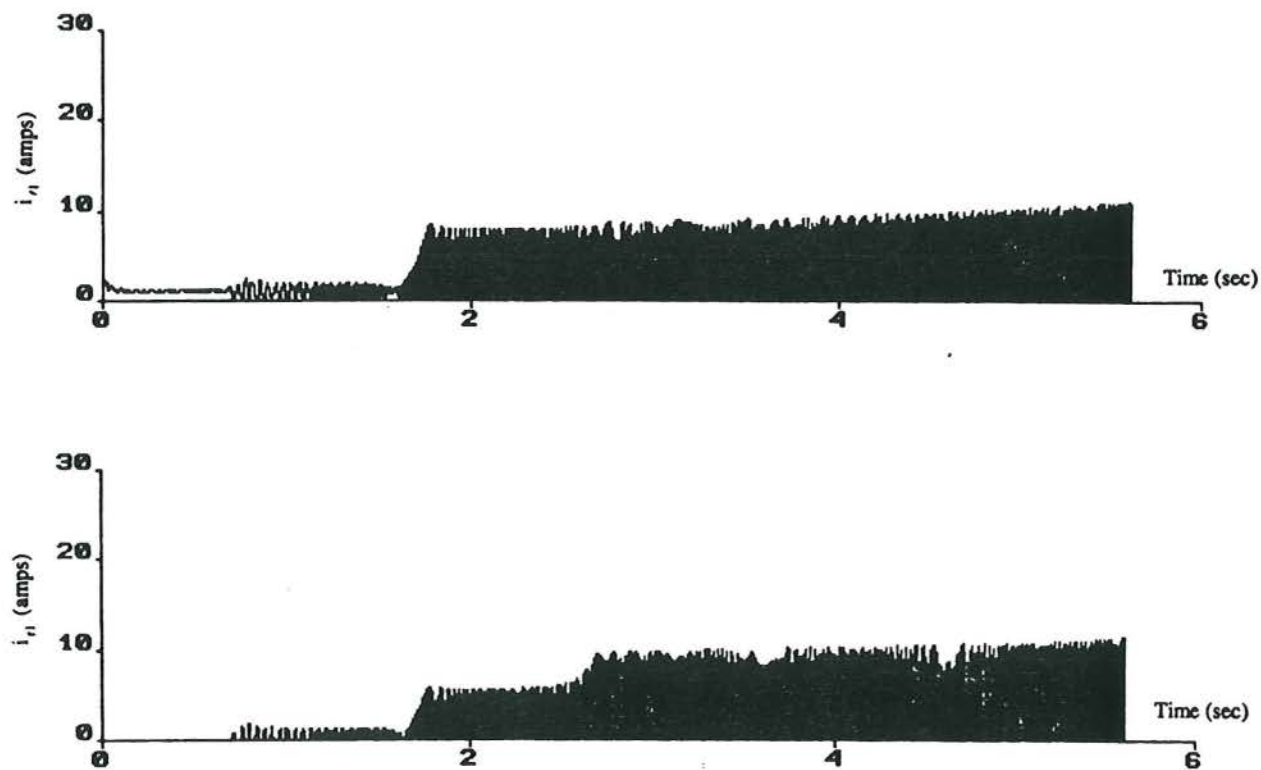
FIGURE 8: TRANSIENT RESPONSE CURRENTS (3-DISK MODEL)
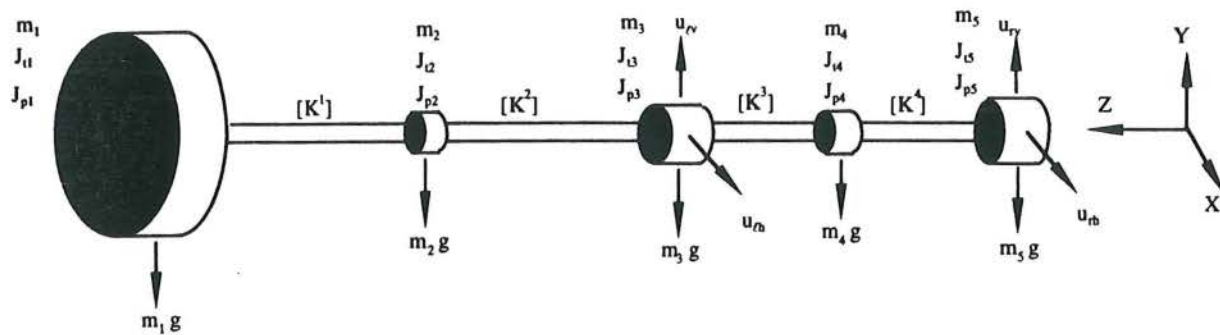
FIGURE 9: 5-DISK MODEL

TRANSIENT RESPONSE (3-DISK MODEL)

This 3-disk, 13 degree-of-freedom model was implemented numerically using a 4th-order Runge-Kutta algorithm with automatic step size adjustment. We deliberately specified an aluminum modulus (see Table 1) in order that the system natural frequencies would remain of manageable magnitude to insure numerical stability without unduly burdensome simulation times. This obviated any need for modal decomposition as might be appropriate in a larger, stiffer model. Also, we chose a linear speed of rotation law to emphasize system critical speeds equally rather than directly employ the first-order dynamics of equation (10). We specified $\ddot{\phi} = 1047 \, \text{rad/sec}^2$ (10000 rpm/sec) commencing at t = .6 sec. The initial condition vector was obtained by solving the static beam deflection problem. That is, we assumed the rotor to be at rest in the bearings with finite gap lengths of 0.3 mm (a reasonable expectation of back-up bearing clearance. Also, we assumed the initial state vector to exhibit nonzero components in the vertical (Y-Z) plane only. The nonzero components of the initial condition vector are given by (in SI units):

$$\underline{x}_0 = [R_{1Y} \; \beta_{1X} \; R_{2Y} \; \beta_{2X} \; R_{3Y} \; \beta_{3X}]^T$$

$$= [-.0039 \; .00994 \; -.0007 \; .00869 \; .0007 \; .00823]^T$$

The transient response curves of the nodes in the Y-Z (vertical) plane are shown in Figure 7, where the abscissa reflects both time and rotational speed. These curves reflect mass unbalance radii with magnitudes of 1% of disk radii, and these selections were purely arbitrary. The first critical speed appears clearly while subsequent critical speeds do not reflect excessive shaft response. The actuator constant K_a (which was specified equally for all electromagnets) is also rather artificial and thus the currents shown in Figures 8 and 9 are simply intended for qualitative interest. We only show the maximum bearing currents, which, in light of the gravitational forces, circulate in the top electromagnet coils of each bearing. The other currents display similar behavior.

5-DISK MODEL

We now concern ourselves with a higher level of sophistication in our model by considering the 5-disk representation illustrated in Figure 9. The mass and inertia of the compliant members is now lumped into conceptual "disks" at the midpoints of the respective shaft spans in straightforward fashion. The relevant nodes which we seek to control are those of the bearing journals at numbers three and five. As before, the homogeneous portion of the model under control action becomes:

$$\begin{bmatrix} [M'] & 0 \\ 0 & [M'] \end{bmatrix} \underline{\ddot{x}} + \begin{bmatrix} [C'_D] & -[C_G] \\ [C_G] & [C'_D] \end{bmatrix} \underline{\dot{x}} + \begin{bmatrix} [K'] & 0 \\ 0 & [K'] \end{bmatrix} \underline{x} = \underline{0} \quad (24)$$
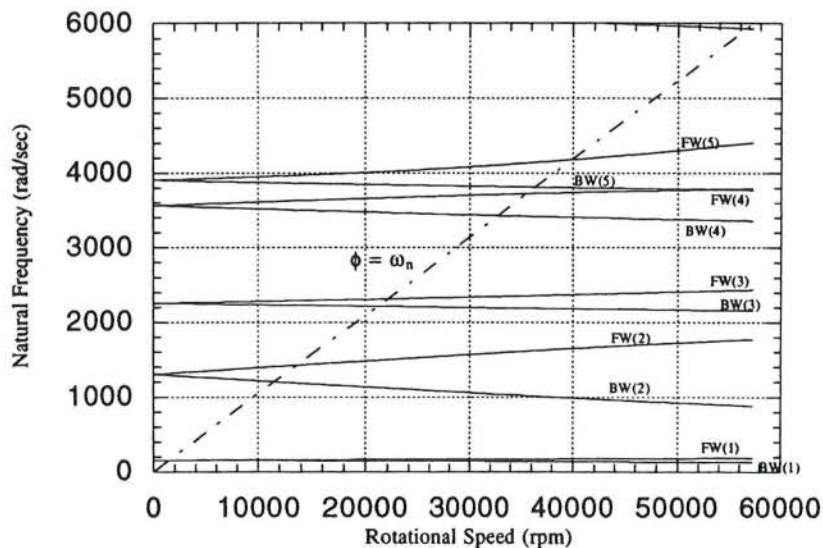

FIGURE 10: CAMPBELL DIAGRAM (5-DISK MODEL)

10

where the component matrices are now 10x10 rather than 6x6 to reflect the additional eight degrees of freedom.

The stiffness component matrix used in equations (24) was the appropriate banded extension of that given in the 3-disk model, but now we have decoupled the 5th, 9th, 15th, and 19th equation in the set of (24).

CONTROLLER DESIGN (5-DISK MODEL)

The input/output feedback linearization controller implicit in the above model was obtained in precisely the same manner as was done with the 3-disk model. That is, the control law(s) for this 5-disk model resembles equations (19):

$$
\begin{aligned}
\mathbf{u}_{\ell v} &= \{\hat{f}_{3Y} + \alpha \dot{R}_{3Y} - m_3 a_{3Y}\dot{\phi}^2 + m_3 a_{3X}\ddot{\phi} + m_3 g\} \\
&\quad + m_3\{c_1\dot{\tilde{g}}_{\ell 1} + c_2\tilde{g}_{\ell 1}\} \\[6pt]
\mathbf{u}_{\ell h} &= \{\hat{f}_{3X} + \alpha \dot{R}_{3X} - m_3 a_{3X}\dot{\phi}^2 - m_3 a_{3Y}\ddot{\phi}\} \\
&\quad + m_3\{c_1\dot{\tilde{g}}_{\ell 3} + c_2\tilde{g}_{\ell 3}\} \\[6pt]
\mathbf{u}_{rv} &= \{\hat{f}_{5Y} + \alpha \dot{R}_{5Y} - m_5 a_{5Y}\dot{\phi}^2 + m_5 a_{5X}\ddot{\phi} + m_5 g\} \\
&\quad + m_5\{c_1\dot{\tilde{g}}_{r1} + c_2\tilde{g}_{r1}\} \\[6pt]
\mathbf{u}_{rh} &= \{\hat{f}_{5X} + \alpha \dot{R}_{5X} - m_5 a_{5X}\dot{\phi}^2 - m_5 a_{5Y}\ddot{\phi}\} \\
&\quad + m_5\{c_1\dot{\tilde{g}}_{r3} + c_2\tilde{g}_{r3}\}
\end{aligned}
\tag{25}
$$

TABLE 3: 5-DISK MODEL PARAMETERS

L_1: .167 m	L_2: .167 m	L_3: .084 m	L_4: .084 m
E_1: 30×10^9 Pa	E_2: 30×10^9 Pa	E_3: 30×10^9 Pa	E_4: 30×10^9 Pa
I_1: 1.4×10^{-9} m^4	I_2: 1.4×10^{-9} m^4	I_3: 1.4×10^{-9} m^4	I_4: 1.4×10^{-9} m^4
m_1: .197 kg	m_2: .062 kg	m_3: .1455 kg	m_4: .031 kg
J_{t1}: .000349 kgm^2	J_{t2}: .000578 kgm^2	J_{t3}: .00033 kgm^2	J_{t4}: .000075 kgm^2
J_{p1}: .000121 kgm^2	J_{p2}: .000001 kgm^2	J_{p3}: .0000088 kgm^2	J_{p4}: .0000005 kgm^2
m_5: .1145 kg	a_{1x}: .000381 m .	a_{1y}: 0 $\quad$ a_{2x}: 0	a_{2y}: 0
J_{t5}: .000042 kgm^2	a_{3x}: −.000127 m	a_{3y}: 0 $\quad$ a_{4x}: 0	a_{4y}: 0
J_{p5}: .00000825 kgm^2	a_{5x}: .000127 m	a_{5y}: 0 $\quad$ c_1: 65	c_2: 1050
α: 1.5 N sec/ m	Δ: .001 m	K_a: 8×10^{-6}	

TABLE 4: 5-DISK MODEL FORWARD AND BACKWARD CRITICAL SPEEDS

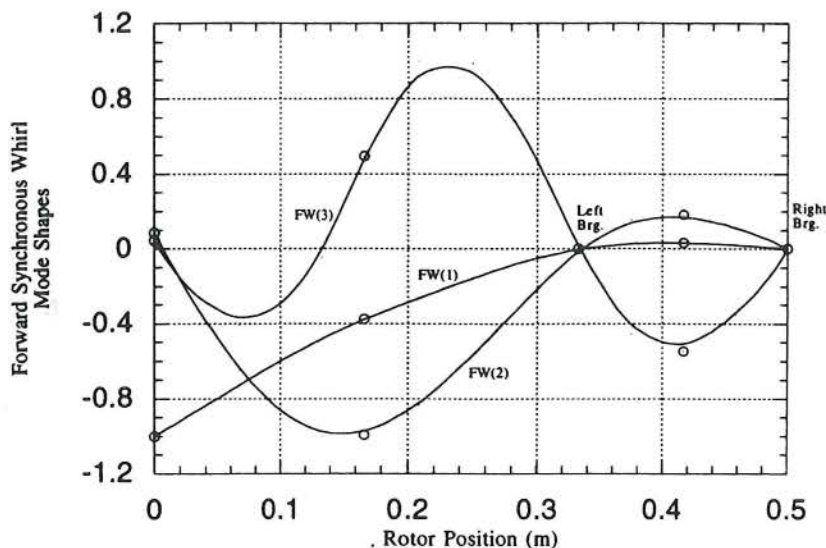| Forward Synchronous Whirl	Backward Synchronous Whirl
ω_{cr1} = FW(1) = 156 rad/sec (1490 rpm)	ω_{cr1} = BW(1) = 154 rad/sec (1471 rpm)
ω_{cr2} = FW(2) = 1424 rad/sec (13,598 rpm)	ω_{cr2} = BW(2) = 1203 rad/sec (11,488 rpm)
ω_{cr3} = FW(3) = 2312 rad/sec (22,078 rpm)	ω_{cr3} = BW(3) = 2212 rad/sec (21,123 rpm)
ω_{cr4} = FW(4) = 3690 rad/sec (35,237 rpm)	ω_{cr4} = BW(4) = 3430 rad/sec (32,754 rpm)
ω_{cr5} = FW(5) = 4220 rad/sec (40,298 rpm)	ω_{cr5} = BW(5) = 3820 rad/sec (36,478 rpm)

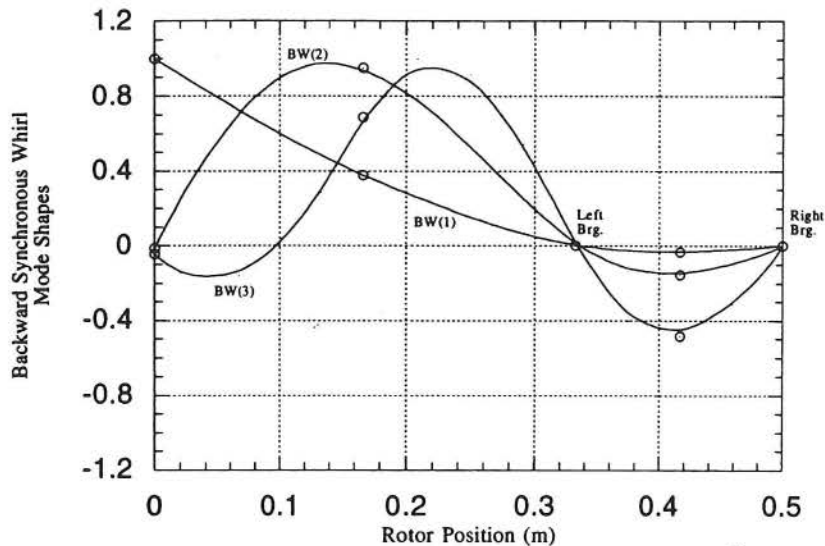FIGURE 11: FORWARD SYNCHRONOUS WHIRL MODE SHAPES (5-DISK MODEL)

FIGURE 12: BACKWARD SYNCHRONOUS WHIRL MODE SHAPES (5-DISK MODEL)

EIGENANALYSIS (5-DISK MODEL)

Proceeding in the manner identical with equation (23), we examine the Y-Z plane of equations (24) and provide the natural frequencies as a function of rotational speed in the Campbell diagram of Figure 10. The parameters used are given in Table 3.

The first five forward and backward synchronous whirl critical speeds are given in Table 4, and the first three forward and backward whirl modes are shown in Figures 11 and 12.

TRANSIENT RESPONSE (5-DISK MODEL)

This 21 degree-of-freedom model was implemented using the same speed of rotation law as the previous model. The nonzero components of the initial condition vector were determined as before by solving the static problem. They are:

$$\underline{x}_0 = [R_{1Y} \ \beta_{1X} \ R_{2Y} \ \beta_{2X} \ R_{3Y} \ \beta_{3X} \ R_{4Y} \ \beta_{4X} \ R_{5Y} \ \beta_{5X}]^T$$

$$= [-.0040 \ .0100 \ -.0020 \ .0100 \ -.0007$$

$$.0090 \ 0.0000 \ .0080 \ .0007 \ .0080]^T$$

12
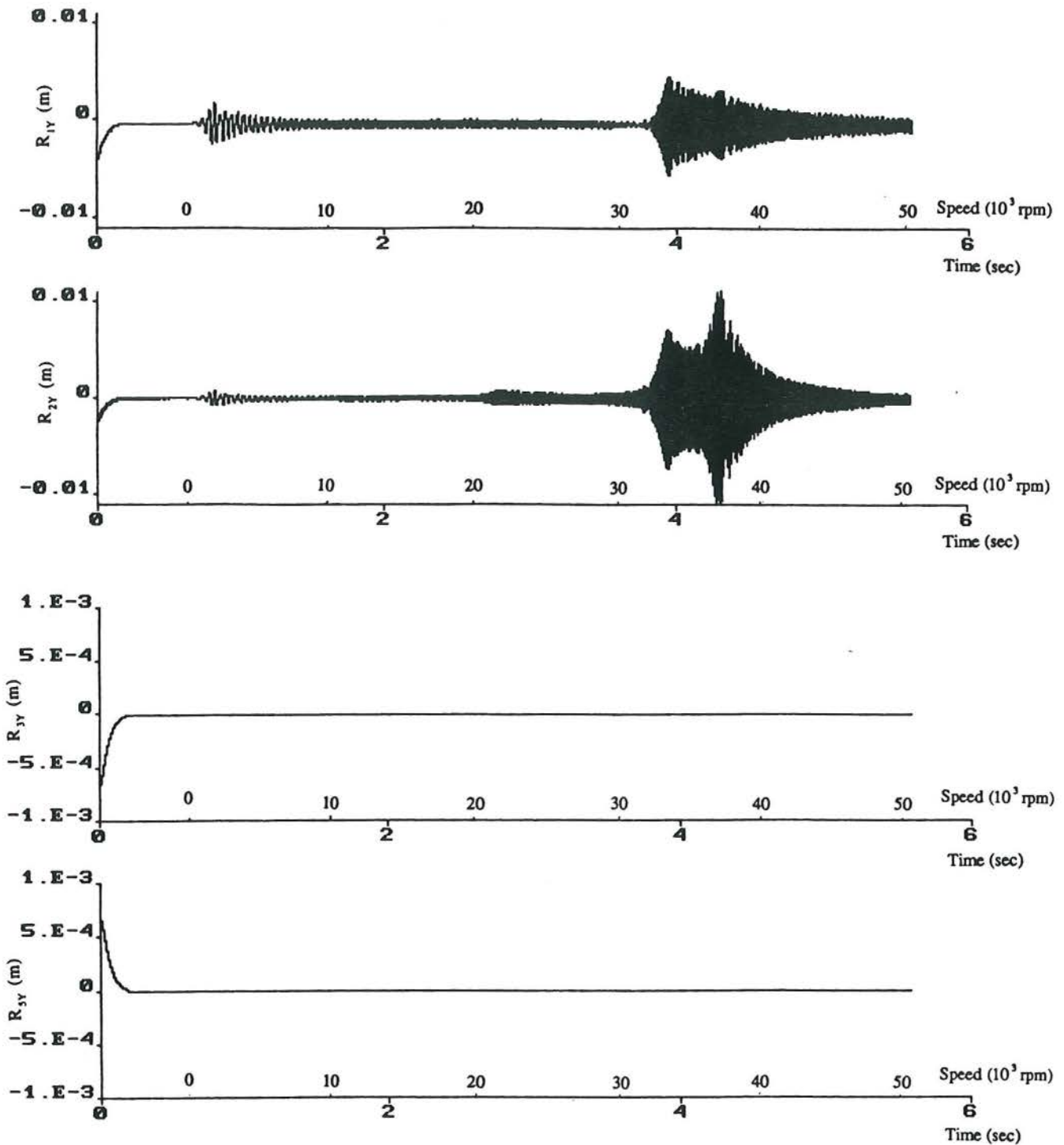
FIGURE 13: TRANSIENT RESPONSE DEFLECTIONS (5-DISK MODEL)

The transient response deflections of the Y-Z plane are given in Figure 13 against both rotational speed and time. We have omitted the deflection of R_{4Y} since it does not reveal any more qualitative information concerning critical speeds than does R_{1Y}, R_{2Y}.

The critical speeds from Table 3 have been noted. The most obvious distinction in Figure 13 is the introduction of excessively flexible vibratory response commencing in the fourth mode. Fortunately, we have a fairly smooth operating range up to about 30000 rpm. One would probably restrict the system's operating speed below the fourth critical.

13
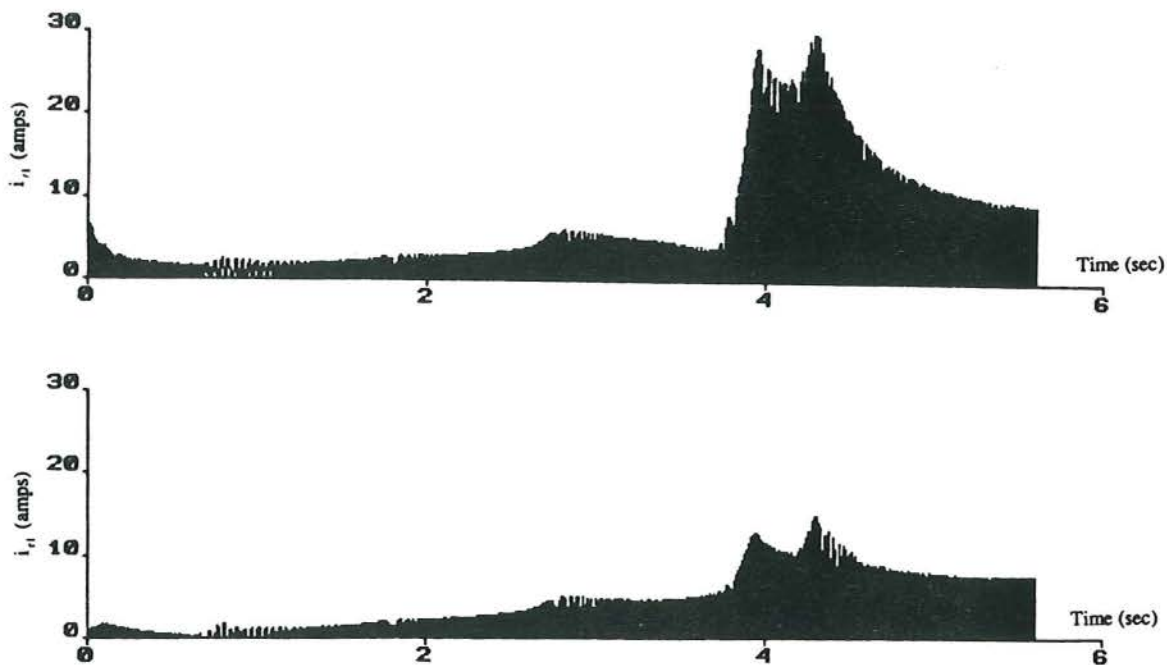
FIGURE 14: TRANSIENT RESPONSE CURRENTS (5-DISK MODEL)

Thus, for the physical system under consideration (Figure 2), the 3-disk model appears to have been satisfactory through the first three modelled natural frequencies. The additional refinement has served to provide a useful upper bound on operating speed. The maximum bearing currents are provided in Figure 14.

ROBUSTNESS AND THE INDEFINITE MODEL

In the none too facetious words of Cellier (1991):

> All too often, simulation is a love story with an unhappy ending. We create a model of a system, and then fall in love with it. Since love is usually blind, we immediately forget all about the experimental frame, we forget that this is *not* the real world, but that it represents the world only under a very limited set of experimental conditions (we become "model addicts").

In that spirit, we pursue considerations of robustness in nonlinear control design, and these have been widely addressed through the so-called sliding mode technique. While we cannot hope to give adequate treatment of the mathematics behind this method here, fairly comprehensive discussions can be found in the literature (Slotine and Li , 1991, Fernandez and Hedrick , 1987, etc.). For example, consider the general n^{th} order, single input system:

$$x^n = f(\underline{x}) + g(\underline{x})u \qquad (26)$$

If x is the scalar output, and $\underline{x} = [x, \dot{x}, \ddot{x}, \dots, x^{(n-1)}]^T$ is the state vector, then the control problem is to force the state $\underline{x}$ to track a specific time-varying state $\underline{x}_d = [x_d, \dot{x}_d, \ddot{x}_d, \dots, x_d^{(n-1)}]^T$ in the face of dynamic uncertainty on $f(\underline{x})$ and $g(\underline{x})$. For the tracking to be achieved without a transient, we must have the initial condition:

$$\underline{x}_d(0) = \underline{x}(0) \qquad (27)$$

We define $\tilde{x} = x - x_d$ as the tracking error, with an appropriate error vector. Now a time-varying surface in the state space is defined by the scalar equation s(x,t) = 0, with

$$s(x,t) = \left(\frac{d}{dt} + \lambda\right)^{n-1} \tilde{x} \qquad (28)$$

where λ is a strictly positive constant. Notice in the development that n equals the number of differentiations of the output variable one must perform in order to retrieve the control input. If, for example, n=2, then equation (28) results in:

$$s = \dot{\tilde{x}} + \lambda\tilde{x} \qquad (29)$$

With the initial condition given by equation (27), tracking $\underline{x} = \underline{x}_d$ is equivalent to remaining on the surface s(x,t) for all t > 0. s = 0 is a linear differential equation whose unique solution is $\tilde{x} = \underline{0}$ given the initial condition of equation (27). Therefore, our control problem becomes that of maintaining s(x,t) = 0. Slotine and Li (1991) demonstrate that if u is chosen such that

$$\frac{1}{2}\frac{d}{dt}s^2 \le -\eta|s| \qquad (30)$$

where η is strictly positive

is satisfied, then our surface will be attractive, and all trajectories of the error vector will be constrained to converge on the surface and remain there. Several types of functions will obey equation (30) (Slotine and Li, 1991, Pradeep and Gurumoorthy, 1993), the classic example of which is the following:
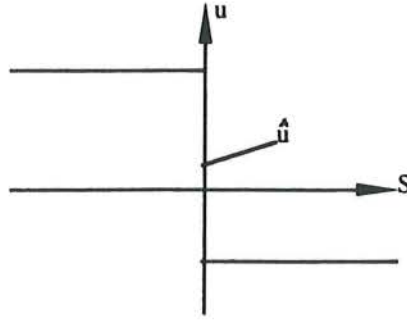
14

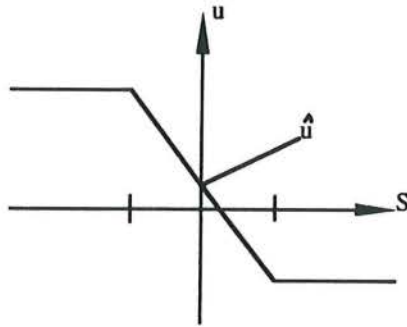FIGURE 15: DISCONTINUOUS CONTROL FUNCTION

FIGURE 16: "SMOOTHED" CONTROL FUNCTION

$$u = \hat{u} - \xi \mathrm{sgn}(s) \qquad (31)$$

where $\hat{u}$ is the nominal control function which cancels the nonlinearities of the nominal model. The form of this function is illustrated in Figure 15. To determine $\hat{u}$, we need only differentiate our surface $s(x,t)$ once. In the example (i.e., n=2),

$$\dot{s} = \ddot{\tilde{x}} + \lambda \dot{\tilde{x}} = \ddot{x} - \ddot{x}_d + \lambda \dot{\tilde{x}} = f(\underline{x}) + g(\underline{x})u - \ddot{x}_d + \lambda \dot{\tilde{x}}$$

and we therefore choose,

$$\hat{u} = \frac{1}{g(\underline{x})}(\ddot{x}_d - \hat{f}(\underline{x}) - \lambda \dot{\tilde{x}}) \qquad (32)$$

where $\hat{f}(\underline{x})$ is the nominal model, and $\left| \hat{f}(\underline{x}) - f(\underline{x}) \right| \le \hat{F}$ is our uncertainty or model error. Substituting this nominal control function into equation (31), and the result into the example plant given by equation (26), we obtain:

$$\frac{1}{2}\frac{d}{dt}s^2 = \dot{s}s = [f(\underline{x}) - \hat{f}(\underline{x}) - \xi \mathrm{sgn}(s)]s$$

$$= (f(\underline{x}) - \hat{f}(\underline{x}))s - \xi|s|$$

Using our expression for the model uncertainty magnitude, and letting $\xi = \hat{F} + \eta$, we obtain:

$$\frac{1}{2}\frac{d}{dt}s^2 \le -\eta|s|$$

In practice, the use of the discontinuous sgn(.) function results in high frequency control activity or chattering (Slotine and Li , 1991). A trade-off is usually made between tracking performance and smooth control such that the sgn(.) function is replaced (for example) by the sat(.) function, where:

sat(.) = (.)   if I(.)I<1

sat(.) = sgn(.)   otherwise

Now the discontinuity has been eliminated, and the control function "smoothed", but at the price of tracking performance. The desired form of the control function now becomes:

$$u = \hat{u} - \xi \mathrm{sat}(s/\Gamma) \qquad (33)$$

where Γ is a boundary layer thickness, as shown in Figure 16. Furthermore, it can be shown that satisfying equation (30) guarantees that if equation (27) is not met exactly, then the surface will still be reached in a finite time smaller than $\left|s(t = 0)\right|/\eta$.
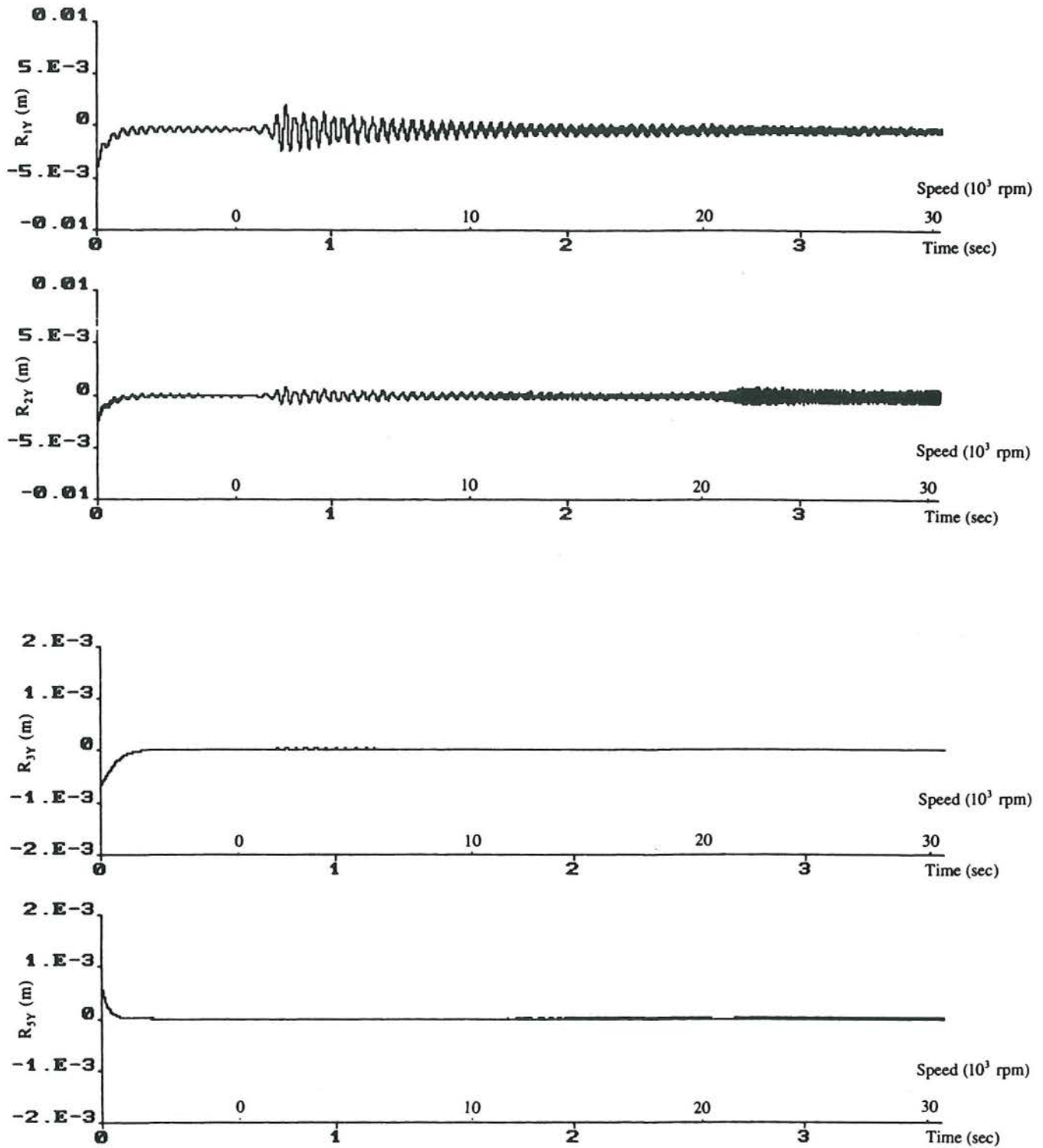
15

FIGURE 17: DISPLACEMENTS OF 5-DISK MODEL USING 3-DISK SLIDING MODE CONTROLLER

16

Returning to our 3-disk model, we define our surfaces as:

$$s_1 = \dot{\tilde{g}}_{\ell 1} + \lambda \tilde{g}_{\ell 1}$$
$$s_2 = \dot{\tilde{g}}_{\ell 3} + \lambda \tilde{g}_{\ell 3}$$
$$s_3 = \dot{\tilde{g}}_{r1} + \lambda \tilde{g}_{r1}$$
$$s_4 = \dot{\tilde{g}}_{r3} + \lambda \tilde{g}_{r3}$$

and differentiate each surface one time in order to recover the control input:

$$\dot{s}_1 = \ddot{\tilde{g}}_{\ell 1} + \lambda \dot{\tilde{g}}_{\ell 1}$$
$$= -1/m_2 \{ -\hat{f}_{2Y} + \alpha \dot{R}_{2Y} + m_2 a_{2Y} \dot{\phi}^2 - m_2 a_{2X} \ddot{\phi} - m_2 g \}$$
$$\quad -(1/m_2) u_{\ell v} + \lambda \dot{\tilde{g}}_{\ell 1}$$

$$\dot{s}_2 = \ddot{\tilde{g}}_{\ell 3} + \lambda \dot{\tilde{g}}_{\ell 3}$$
$$= -1/m_2 \{ -\hat{f}_{2X} + \alpha \dot{R}_{2X} + m_2 a_{2X} \dot{\phi}^2 + m_2 a_{2Y} \ddot{\phi} \}$$
$$\quad -(1/m_2) u_{\ell h} + \lambda \dot{\tilde{g}}_{\ell 3}$$

$$\dot{s}_3 = \ddot{\tilde{g}}_{r1} + \lambda \dot{\tilde{g}}_{r1}$$
$$= -1/m_3 \{ -\hat{f}_{3Y} + \alpha \dot{R}_{3Y} + m_3 a_{3Y} \dot{\phi}^2 - m_3 a_{3X} \ddot{\phi} - m_3 g \}$$
$$\quad -(1/m_3) u_{rv} + \lambda \dot{\tilde{g}}_{r1}$$

$$\dot{s}_4 = \ddot{\tilde{g}}_{r3} + \lambda \dot{\tilde{g}}_{r3}$$
$$= -1/m_3 \{ -\hat{f}_{3X} + \alpha \dot{R}_{3X} + m_3 a_{3X} \dot{\phi}^2 + m_3 a_{3Y} \ddot{\phi} \}$$
$$\quad -(1/m_3) u_{rh} + \lambda \dot{\tilde{g}}_{r3}$$

Thus, we shall choose our control functions as:

$$u_{\ell v} = \{ \hat{f}_{2Y} + \alpha \dot{R}_{2Y} - m_2 a_{2Y} \dot{\phi}^2 + m_2 a_{2X} \ddot{\phi} + m_2 g \}$$
$$\quad + m_2 \lambda \dot{\tilde{g}}_{\ell 1} + m_2 \xi_1 \mathrm{sat}(s_1 / \Gamma)$$

$$u_{\ell h} = \{ \hat{f}_{2X} + \alpha \dot{R}_{2X} - m_2 a_{2X} \dot{\phi}^2 - m_2 a_{2Y} \ddot{\phi} \}$$
$$\quad + m_2 \lambda \dot{\tilde{g}}_{\ell 3} + m_2 \xi_2 \mathrm{sat}(s_2 / \Gamma)$$

$$u_{rv} = \{ \hat{f}_{3Y} + \alpha \dot{R}_{3Y} - m_3 a_{3Y} \dot{\phi}^2 + m_3 a_{3X} \ddot{\phi} + m_3 g \} \quad (34)$$
$$\quad + m_3 \lambda \dot{\tilde{g}}_{r1} + m_3 \xi_3 \mathrm{sat}(s_3 / \Gamma)$$

$$u_{rh} = \{ \hat{f}_{3X} + \alpha \dot{R}_{3X} - m_3 a_{3X} \dot{\phi}^2 - m_3 a_{3Y} \ddot{\phi} \}$$
$$\quad + m_3 \lambda \dot{\tilde{g}}_{r3} + m_3 \xi_4 \mathrm{sat}(s_4 / \Gamma)$$

where substitution reveals $\dot{s}_i = -\xi_i \mathrm{sat}(s_i / \Gamma)$ which satisfies equation (30), thus guaranteeing attractive surfaces.

The control law(s) specified in equations (34) were implemented on the 5-disk model to serve as a brief example of unmodelled dynamics. This is shown in Figure 17. The sliding mode controller parameters were chosen (equally) as:

$$\xi : 4000$$
$$\lambda : 40$$
$$\Gamma : .05$$

and the rotor was accelerated through 30000 rpm, as we are not interested in the excessively vibratory modes beyond this speed (refer Figure 13). Although we have removed the restriction of the bearing journals remaining at zero displacement (i.e., nominal gap length), the above choice of controller parameters displays similar behavior as the 5-disk model "perfect controller".

CONCLUSIONS

For the purists who object to our lumped parameter models, we will briefly touch on the ramifications of the finite element description of the flexible rotor. Consider the general multiple degree-of-freedom system:

$$[M]\ddot{\underline{x}} + [C_G + C_D]\dot{\underline{x}} + [K]\underline{x} = \underline{F} \quad (35)$$

where all matrices are nondiagonal, and [K] is as previously defined. Owing to coupling in the highest derivatives implied in a nondiagonal mass matrix, we will recover second-order derivatives of the states when we differentiate our gap length errors (as in the I/O controller development). If one initially multiplies equation (35) by $[M]^{-1}$, we can diagonalize the mass matrix, but this couples control action in our other state equations, and one will be led to solve for the control functions (as in equations (19), (25)) simultaneously, rather than directly. We see

$$[I]\ddot{\underline{x}} + [M]^{-1}[C_G + C_D]\dot{\underline{x}} + [M]^{-1}[K]\underline{x} = [M]^{-1}\underline{F} \quad (36)$$

such that $\ddot{\tilde{g}}_{\ell 1}$, which may be written as $-\ddot{R}_{2Y}$ in the 3-disk model, now contains all control functions (for a full mass matrix), as do the other gap length errors, since the row corresponding to the coordinate R_{2Y} will contain some appropriate linear combination of all the elements of $\underline{F}$. It was in the interest of avoiding this mathematical inconvenience that we pursued the lumped parameter representation of our system.

It will be recalled from the definitions of the elastic forces appearing in the 3-disk controller equations, that we are feeding back the coordinates of the adjacent nodes of our bearing journal in our nonlinear cancellation. Thus, in the 3-disk model, the left bearing journal control requires position and angle information from the "end disk". In contrast, the 5-disk model controller required measurement of the coordinates of the shaft mid-span "points", and needless to say, one may be more convenient than the other. Of course, this remains within the context of compensation without the use of an effective observer. We defer to a later date any discussion of nonlinear observers, etc.

We deliberately avoided any treatment regarding modal decomposition of rotordynamic systems by postulating a sufficiently flexible rotor. Also, we recognize that the fourth-order Runge-Kutta algorithm is not necessarily the best approach for numerically stiff systems. We are encouraged by the recent progress in "stiff integrator" algorithms, and all computational output has been duplicated using the DVODE software.

Pradeep and Gurumoorthy (1993), have treated many other effective nonlinear controller schemes, at least within the context of the *rigid* rotor. Our primary interest has been in elucidating the general structure of such discontinuous controllers as the sliding mode method, within the framework of flexible rotordynamics. We have avoided the consideration of voltage-driven actuators to simplify matters, and we shall defer that topic to a later date as well.
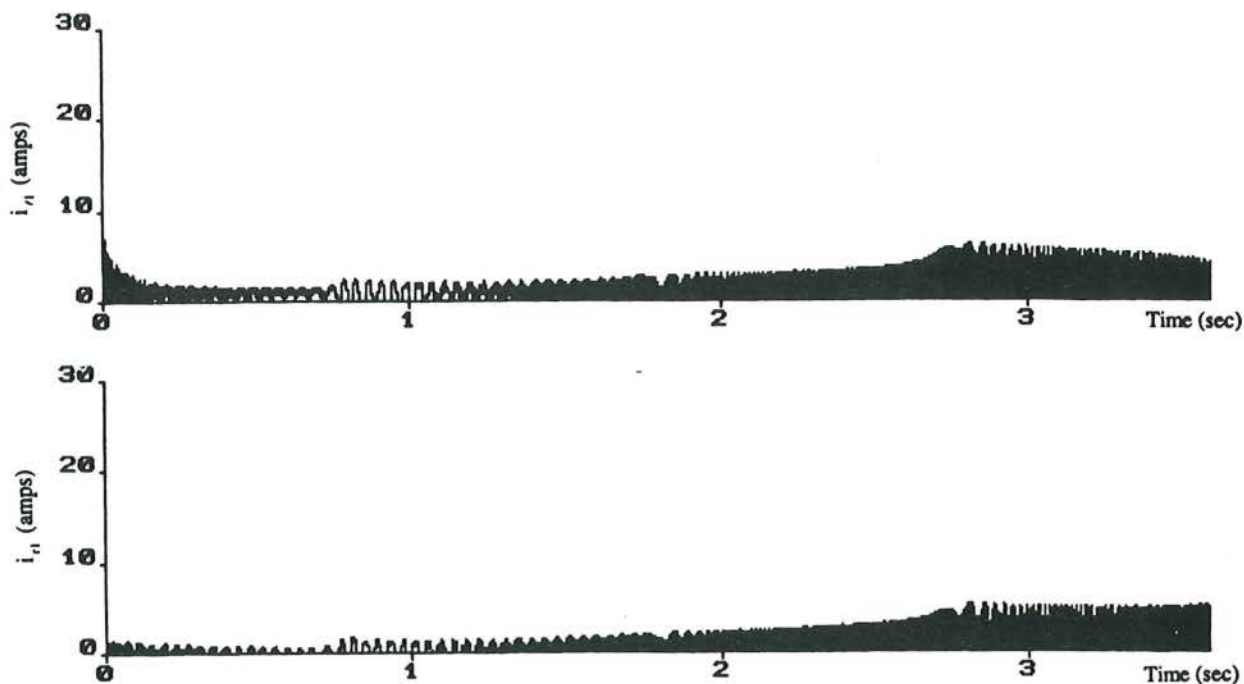
FIGURE 18: CURRENTS FOR 3-DISK SLIDING MODE CONTROLLER IMPLEMENTED ON 5-DISK MODEL

We do not wish to leave the impression that uncertainty in the model of the flexible rotor itself (as in our treatment) is necessarily the justification for effectively robust controllers. More realistically, one might be concerned with models of the fluid interaction forces, intermittent rotor/stator contact models, structural damping, etc., and it is these indefinite features of the rotordynamic problem which one might be interested in accommodating.

ACKNOWLEDGEMENTS

REFERENCES

[1] Burrows, C.R., N. Sahinkaya, A. Traxler, and G. Schweitzer, "Design and Application of a Magnetic Bearing for Vibration Control and Stabilization of a Flexible Rotor", *Magnetic Bearings*, Proceedings of the First International Symposium, ETH Zurich, Switzerland, June 1988.

[2] Cellier, Francois E., *Continuous System Modeling* , 1991, Springer-Verlag.

[3] Childs, D., *Turbomachinery Rotordynamics: Phenomena, Modeling, & Analysis*, 1993, John Wiley & Sons.

[4] Fernandez R., Benito, and J. Karl Hedrick, "Control of multivariable non-linear systems by the sliding mode method", *International Journal of Control*, Vol. 46, No. 3, pp. 1019-1040, 1987.

[5] Geary, P.J., "Magnetic and Electric Suspensions", SIRA Research Report R314, British Scientific Research Association, 1964.

[6] Genta, G., *Vibration of Structures and Machines* , 1993, Springer-Verlag.

[7] Hebbale, K. V., "A Theoretical Model for the Study of Nonlinear Dynamics of Magnetic Bearings", Ph. D. Dissertation, Cornell Univ., January 1985.

[8] Humphris, R.R., "A Bibliography on Magnetic Bearings", Report No. UVA/643092/MAE85/336, Univ. of Virginia, 1985.

[9] Humphris, R.R., R. D. Kelm, D. W. Lewis, and P. E. Allaire, "Effect of Control Algorithms on Magnetic Journal Bearing Properties", *Journal of Engineering for Gas Turbines and Power*, Vol. 108, pp. 624-632, October 1986.

[10] Johnson, B. G., "Active Control of a Flexible Two-Mass Rotor Suspended in Magnetic Bearings", presented at the 11th Biennial ASME Design Engineering Conference on Vibration and Noise, Boston, MA, September 1987.

[11] Kailath, T., *Linear Systems*, 1980, Prentice-Hall.

[12] Lalanne, M., and G. Ferraris, *Rotordynamics Prediction in Engineering*, 1990, John Wiley & Sons.

[13] Maslen, E.H., "Magnetic Bearing Synthesis for Rotating Machinery", Ph. D. Dissertation, Univ. of Virginia, January 1991.

[14] Maslen, E.H., and P. E. Allaire, "Magnetic Bearing Sizing for Flexible Rotors", *Journal of Tribology*, Vol. 114, pp. 223-229, April 1992.

[15] Pradeep, A. K., and R. Gurumoorthy, "Nonlinear Control of Magnetic Bearings", General Electric Company, Magnetic Suspension Technology, Proceedings of the 2nd International Symposium, Seattle, WA, August, 1993.

[16] Raghavan, S., and J. Karl Hedrick, "Sliding Compensators for a Class of Nonlinear Systems", Proc. of ACC, San Diego, CA, pp. 1174-1178, 1990.

[17] Raghavan, S., "Observers And Compensators For Nonlinear Systems, With Application To Flexible-Joint Robots", Ph. D. Dissertation, Univ. of California at Berkeley, January 1992.

[18] Salm, J., and G. Schweitzer, "Modeling and Control of a Flexible Rotor with Magnetic Bearings", Conference Proceedings on Vibrations in Rotating Machinery, Inst. Mech. Eng., York, UK, September 1984.

[19] Salm, J.R., "Active Electromagnetic Suspension of an Elastic Rotor: Modeling, Control, and Experimental Results", presented at the ASME Design Engineering Division Conference on Vibration and Noise, Boston, MA, September 1987.

[20] Slotine, Jean-Jacques, J. K. Hedrick, and E. A. Misawa, "On Sliding Observers for Nonlinear Systems", *Journal of Dynamic Systems, Measurement, and Control*, Vol. 109, pp. 245-252, September 1987.

[21] Slotine, Jean-Jacques, and Weiping Li, *Applied Nonlinear Control*, 1991, Prentice-Hall.

[22] Sortore, C.K., "Design of Permanent Magnet Biased Magnetic Bearings For a High Speed Rotor", M.S. Thesis, Univ. of Virginia, January 1990.

[23] Woodson, H.H., and J. R. Melcher, *Electromechanical Dynamics Part 1: Discrete Systems*, 1990 Reprint Ed., Krieger.

[24] Yoshimoto, T., "Eddy Current Effect in a Magnetic Bearing Model", *IEEE Transactions on Magnetics*, Vol. MAG-19, No. 5, pp. 2097-2099, September 1983.